

A planet on an inclined orbit as an explanation of the warp in the β Pictoris disk

D. Mouillet¹J.D. Larwood²J.C.B. Papaloizou²A.M. Lagrange¹¹ *Laboratoire d'Astrophysique de l'Observatoire de Grenoble, UMR 5571, Université J. Fourier, BP 53, F-38041 Grenoble Cedex 9*² *Astronomy Unit, School of Mathematical Sciences, Queen Mary & Westfield College, Mile End Road, London E1 4NS*

Received: ; accepted:

ABSTRACT

We consider the deformation that has recently been observed in the inner part of the circumstellar disk around β Pictoris with the HST. Our recent ground based adaptive optics coronagraphic observations confirm that the inner disk is warped. We investigate the hypothesis that a yet undetected planet is responsible for the observed warp, through simulations of the effect of the gravitational perturbation due to a massive companion on the disk. The physical processes assumed in the simulations are discussed: since the observed particles do not survive collisions, the apparent disk shape is driven by the underlying collisionless parent population. The resulting possible parameters for the planet that are consistent with the observed disk deformation are reviewed.

Key words: stars: individual: β Pictoris – circumstellar matter – planetary systems.

1 INTRODUCTION

An important discovery by IRAS was the detection of IR excess due to cold material around a number of Main Sequence Stars. Among them, β Pictoris exhibits one of the largest excess (Aumann, 1985). Shortly after the IRAS results, a disk of dust was imaged around this star (Smith and Terrile, 1984). Since then, the disk has been extensively studied, as it is expected to be related to planetary systems, possibly in a state of evolution different from that of our Solar System.

The disk composition is complex. Micron sized grains are detected through scattered light (Kalas and Jewitt, 1995 and ref. therein; Mouillet et al, 1996) and thermal emission (Lagage and Panin, 1994). The presence of small amounts of submicron grains is inferred from 10 μm spectrophotometry (Knacke et al, 1993). Larger grains (mm sized) are detected through photometry at mm wavelengths (Chini et al, 1991; Zuckerman and Becklin, 1993). Kilometer-sized bodies have also been proposed to account for the very peculiar spectroscopic variability of β Pictoris (Lagrange et al, 1987). Gas is detected spectroscopically through the presence of absorption lines. However the gas to dust ratio is probably ≤ 1 , ie much less than that in the environment of young stars

such as T Tauri, or in star forming regions. Most of the gas is probably confined very close to the disk (Lagrange, 1995 and ref. therein).

The total mass of the disk is very uncertain as most of it comes from the largest bodies. About one Earth Mass is necessary to account for optical to mm observations. If the particle size distribution follows a law of the form,

$$dn(a) \propto a^{-3.5} da,$$

with $n(a)$ being the number of particles of size greater than a , up to kilometer size bodies, the mass would be several tens of Earth Masses (Backman and Paresce, 1993).

The origin and evolution of this system is still the subject of active research and one point of investigation is the possible presence of planets within the disk. From the theoretical point of view, planets are expected to be formed out of the the circumstellar disk that accompanies the star during the process of formation. The timescale estimated for this process (see Lin and Papaloizou, 1985) is characteristically less than the estimated lifetime of β Pictoris $\sim 2.10^8 y$ (Paresce, 1991). Thus it is reasonable to suppose that planets have had time enough to form.

Obtaining direct evidence for the existence of planets around early type stars such as β Pictoris is far from

straightforward. Direct imaging is still beyond current observational capability because of the high contrast between the star and the planet. Photometric variations have been observed (Lecavelier et al, 1995) which are consistent with the occultation of β Pictoris by an orbiting Jupiter-like planet. But this has not been firmly established (observation of another occultation is needed to sweep all doubts away). Radial velocity studies, such as those performed to detect giant planets around solar type stars such as 51 Peg, 47 UMa, and others (Mayor and Queloz, 1995, Marcy and Butler, 1996) would not provide enough accuracy to detect giant planets at distances of about a few AU from these usually rapidly rotating early type stars.

Signatures of planets can result from their gravitational effect on the disk. The observed clearing of the inner region of the disk has been attributed to the gravitational effect of an orbiting planet (Roques et al, 1994). But other physical processes can explain the observed dust distribution as well.

The gravitational influence of a planet has been invoked in order to explain the observed high rate of cometary infall (about 1000 per year corresponding to $\sim 10^{-15} M_{\odot} y^{-1}$). Beust and Morbidelli (1995) propose that mean motion resonances between the orbits of kilometer sized bodies and a planet in a longer period eccentric orbit can produce the right quantity, and orbits of infalling bodies. They predict long term variabilities which are currently being tested via a spectroscopic survey. Such a model requires a steady flux of kilometer sized bodies from the outer to inner regions of the disk to occur as a consequence of collisions.

Finally, HST data provide high S/N data on the light scattered from the the inner part of the disk down to 25 AU from the star (Burrows et al, 1995). They revealed a slight inclination (~ 3 degrees) of the inner disk midplane up to about 50 AU, to the outer disk midplane. Burrows et al (1995) proposed that a planet on an orbit inclined to the outer disk plane might be the most probable explanation for this observation. In section 2, we show recent ground-based observations imaging the same region of the disk for comparison. In section 3 we review the physical properties of the disk to determine how an hypothetical planet would act on it. This leads to 3-D numerical simulations of the simultaneous behaviour of large numbers of test particles representing a disk population of kilometer sized objects under the gravitational field of the star and massive companion on an inclined, and possibly eccentric orbit. In section 4 we present the results. We finally discuss the possible parameters for the companion consistent with its presence being able to explain the brightness asymmetry of the inner β Pictoris disk.

2 OBSERVED ASYMMETRY OF THE INNER PART OF THE β Pictoris DISK

2.1 Adaptive optics observations of the inner disk

No warp has been detected in the classical coronagraphic observations outside 80 AU. In order to observe the disk closer to the star, one needs high angular resolution observations, ie either space observations or atmospheric effect corrected images. Recently, adaptive optics coronagraphic images of the β Pictoris disk enabled us to detect the disk in the near infrared (NIR) through scattered light down to about 25

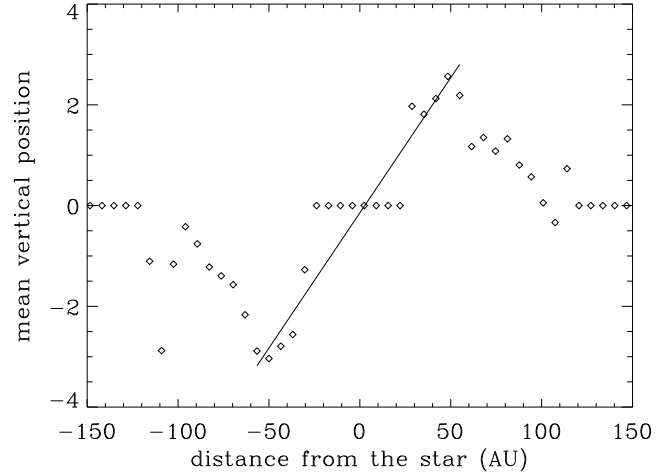


Figure 2. The observed vertical deformation of the disk above the outer disk midplane. The axes are marked in AU. The vertical deformation is measured from the centroid of the brightness distribution in the direction normal to the outer disk midplane. The value zero is adopted when the measurement is not possible (closer than 25 AU and further than 110 AU). The solid line is the linear fit for the inner part. We define the extent of the deformation as the distance at which the slope of the fit starts to decrease. The extent of the deformation is 50 AU, and the corresponding inclination 3 degrees

AU from the star (Mouillet et al, 1996). Similar resolution was obtained with HST in the optical range (Burrows et al, 1995).

We performed new observations of the β Pictoris disk with a coronagraph coupled to the ESO adaptive optics system ADONIS on January 5, 1996 in the J band (Fig. 1). The inner region (30-80 AU) is observed with an angular resolution similar to that of HST. However, the correction for atmospheric turbulence makes it more difficult to subtract perfectly the stellar light which remains after the mask, so that some residuals of the PSF temporal variations remain on the image. Details of the observing method and of the reduction procedure can be found in Beuzit et al (1996).

From Fig.2 we see that the intensity peak lies on one of two lines according to whether it is nearer or further than 50 AU from the centre. Thus the disk midplane inside 50 AU is inclined at about 3 degrees to the outer disk midplane. The effect of the warp is hardly seen, but nonetheless it is consistent with the HST data in terms of amplitude and extent.

These observations confirm previous results (Mouillet et al, 1996; Burrows et al, 1996): the surface brightness profile $I(r)$, which is measured to be very steep far from the star (Kalas and Jewitt, 1995), gets flatter and flatter as the distance to the star, r , decreases from 100 AU down to 25 AU. For $r > 100$ AU, $I(r) \propto r^{-3.5}$. For $50 \text{ AU} < r < 100$ AU, $I(r) \propto r^{-1.3}$. For $r < 50$ AU, the profile is even flatter. (Fig. 3). Consequently, the form of the optical optical depth as a function of r , given by $\tau(r) = 5 \cdot 10^{-3} (r/100)^{-1.7}$, which is valid for $r > 100$ AU, cannot be used for smaller values of r . The inferred form depends on the precise model involving a combination of thermal IR and scattering observations, but it converges on a progressive flattening up to a maximum value of 10^{-3} - 10^{-2} at around $r = 40$ AU, thereafter de-

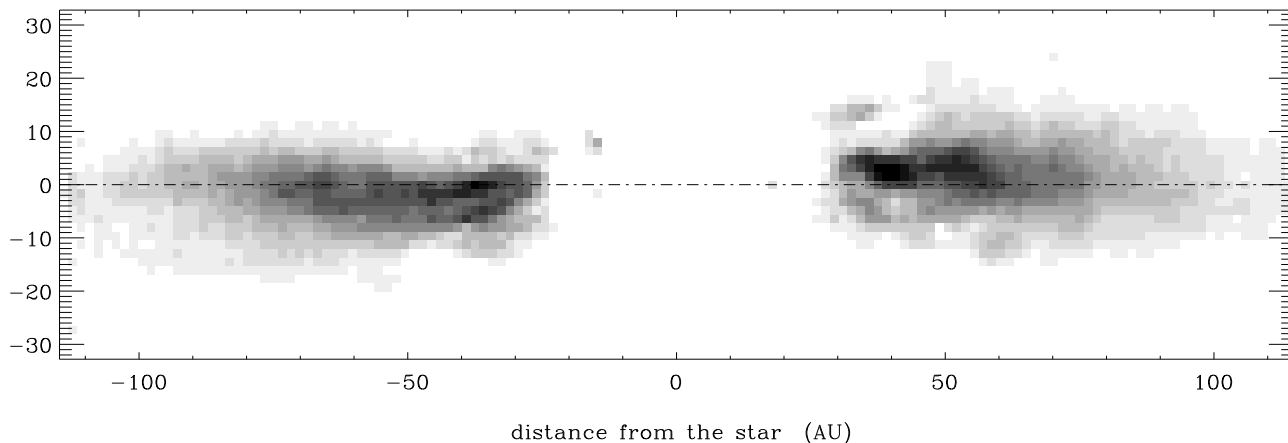


Figure 1. Adaptive optics observations in the J band of the inner disk of β Pictoris, January 05 1996. The axes are marked in AU. Inward of 50 AU, the disk midplane is inclined with respect to the outer disk midplane (dashed line)

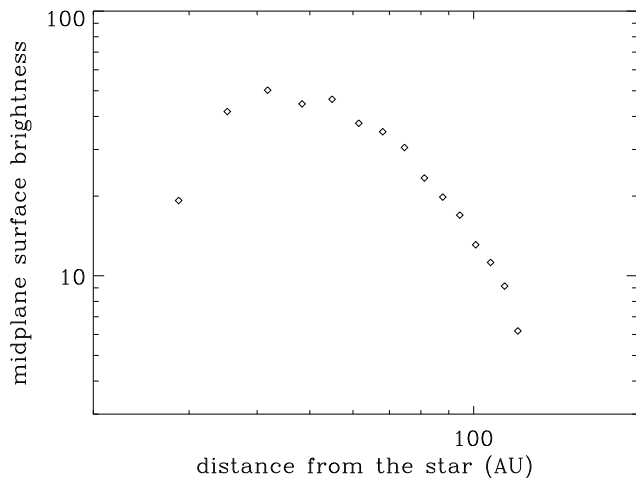


Figure 3. Midplane surface brightness of the disk

creasing inwards. Very little residual dust is expected closer than 15 AU, since it would induce IR excesses in NIR which are not observed.

2.2 The planetary hypothesis

The deformation of the inner disk midplane relative to the outer disk midplane is not the only asymmetry observed in the β Pictoris disk (Kalas and Jewitt 1995; Lagage and Pantin, 1994). All these asymmetries are difficult to explain in the context of a low mass disk consisting of many small objects under a dominant potential arising from a central point mass, since any azimuthal inhomogeneities would be expected to disappear on an orbital timescale (a few 1000 years at 100 AU). A single physical process is unlikely to be responsible for all of them since very different spatial scales are involved together with different geometries. For instance, anisotropic scattering properties together with a slightly inclined disk were proposed to explain the so called “butterfly” asymmetry (Kalas and Jewitt, 1995: the midplane is not an axis of symmetry of the brightness distribution). But such an explanation is unable to count for any radial-dependent asymmetry. Another idea is that the local

production of very small grains as collision products followed by their efficient acceleration by radiation pressure could produce catastrophic blow out in some random part of the disk (Artymowicz, 1996). Such a mechanism could explain any kind of asymmetry without the need of a planet. But the strong antisymmetry (global azimuthal structure) of the observed warping with respect to the central star make this an implausible explanation for it. In this paper we investigate the possibility that the warping asymmetry is produced by an as yet undetected planet in order to see what constraints might be put on its parameters. Although we are not able to claim this as a unique explanation, we are able to show that the required parameters are reasonable and not at present in conflict with constraints arising from the lack of observational detection through either imaging or spectroscopy.

3 NUMERICAL SIMULATIONS OF THE INFLUENCE OF A PLANET

3.1 Physical processes in the β Pictoris disk

The dynamics in the disk is dominated by the gravitational force of the central star to which may be added effects due to any possible perturbing planets. The mass of observed disk material is negligible. Radiation pressure is important for small grains less than a characteristic size $a_c = 2\mu\text{m}$ (Artymowicz, 1988). For such grains the force due to radiation pressure exceeds gravity so that they are on unbound hyperbolic orbits. Accordingly their lifetime is on the order of the crossing time of the disk and thus very short. The Poynting Robertson effect is negligible as is gas drag due to the small quantity of gas present (Artymowicz, 1995).

The main quantity determining the grain collision frequency is the optical depth of the dust, τ . The mean time between collisions is given by

$$t_c = \frac{P_{ORB}}{\pi\tau},$$

where P_{ORB} is the local orbital period. For the β Pictoris disk, the optical depth has been estimated to be typically 5×10^{-3} for small size scattering particles. Supposing that the particle size distribution is given by

$dn(a) \propto a^{-3.5} da$, (which might arise from collision processes) the smallest micron sized grains contribute most of the optical depth. The collision time at 100AU is then typically $10^5 y$ for such grains. The characteristic impact velocities are $\sim v_r = iv_{orb} \sim 1 km/s$, where v_{orb} is the orbital velocity and i is a characteristic inclination in radians associated with a grain orbit. The expected impact velocities are sufficient to destroy the colliding particles. Therefore the lifetime of the smallest particles in bound orbits is on the order of the collision time $\sim 10^5 y$ at 100 AU and even shorter closer than 100 AU, in any case much less than the age of the system. Thus they need to be replenished by the destruction of larger particles. For normal solid state densities, the surface density of disk material contained in small particles is $\Sigma \sim a_c \tau$, which implies a mass of $\sim 10^{-9} M_\odot$ contained within 100AU, and a mass loss rate of around $10^{-14} M_\odot y^{-1}$.

Assuming that collisions will determine both the particle size distribution through fragmentation processes ($dn(a) \propto a^{-3.5} da$) as well as the particle lifetimes, most of the mass in the system will reside in the largest bodies which also contribute least to the optical depth. It is natural to regard the larger bodies, as a primary source of material to drive the global mass loss rate of the system. After a (destructive) collision, the particle ejection velocities, as viewed in the centre of mass frame, are negligible compared to the orbital velocity of the parent particles. Consequently, the global distribution of any given size particles is not driven by interaction processes but is closely related to that of the much bigger parent bodies. This means that the disk shape of the small particles detected in scattered light is driven by the kinematic effect of gravitation on long-lived (old as the system) particles .

Because of the detection of this disk, the collision time of the biggest bodies is expected to be larger than the age of the system. As an illustrative example, if the largest sized bodies are km sized, the given size distribution indicates that $\sim 3.10^{-5} M_\odot$ should be contained in these bodies and the characteristic collision time between them to be $\sim 3.10^9 y$. If a significant amount of the material involved in collisions ends up in small particles, then the supply rate could be as much as $\sim 10^{-14} M_\odot y^{-1}$. Note too that collisions between the km sized bodies also result in an inward radial migration of the distribution much as for viscous accretion disks or planetary rings. The effective diffusion coefficient is $D_c \sim H^2/t_c$, H being the vertical thickness and t_c being the collision time. For $H = 0.1r$, and $t_c = 10^9 y$, this gives a diffusion timescale of $r^2/D_c \sim 10^{11} y$, corresponding to a mass flow rate of $\sim 3.10^{-16} M_\odot y^{-1}$. Apart from lifetime considerations, a large number of such km sized bodies is expected in the β Pictoris disk to explain the spectroscopic detection of highly redshifted variable gas close to the star (Beust et al. 1996). Were even larger bodies to exist around the star, like the kilometer sized objects they might also provide a source of small particles, but they would be expected to have a similar or perhaps even longer effective collision frequency, and thus behave in a similar way from the point of view of our analysis.

Accordingly we model the disk as a system containing a large number of long-lived objects, which as far as the majority is concerned, are collisionless. We then suppose that, as they do not survive more than one collision, the small particles reflect the distribution of the large bodies. We are

Table 1. Parameter sets of the simulations in model units (see text)

Model	M/M_\star	D	e	i	Run time
01	1e-3	1.	0.	3	1e5
02	4e-3	0.5	0.	3	1e5
03	9e-3	0.33	0.	3	3e5
04	5e-3	1.	0.	3	1e5
05	1e-2	0.7	0.	3	1e5
06	1e-2	1.	0.	3	1e5
07	1e-3	0.7	0.1	3	7.5e5
08	1e-3	0.7	0.3	3	3e5
09	1e-3	0.7	0.5	3	3e5
10	1e-2	0.7	0.1	3	3e5
11	1e-2	0.7	0.3	3	3e5
12	1e-2	0.7	0.5	3	3e5
12b	1e-2	0.7	0.5	6	3e5

thus concerned with kinematic patterns produced by non-interacting particles.

3.2 Numerical simulations

The numerical simulations are based on a collisionless adaptation of the SPH code described in Larwood and Papaloizou (1997, and references therein). In this version pressure and viscous forces are removed so that we consider a purely kinematic model. The code follows the velocity and position coordinates of typically 15,000 particles over thousands of revolutions of the perturbing companion. The particles were initially set up in circular motion in a disk configuration with aspect ratio $H/r = 0.1$. They were inserted, using a random number generator according to the following Σ distribution (in model units) to schematically represent the matter distribution in the β Pictoris disk (since the particles are collisionless, the precise form of $\Sigma(r)$ has no effect on the amplitude and extension of the consequent warp):

- for $1.2 \leq r \leq 4.2$, $\Sigma(r) \propto r^{-0.5}$
- for $4.2 \leq r \leq 6$, $\Sigma(r) \propto r^{-1.5}$.

The model unit of length corresponding to $r = 1$, R_{unit} , is arbitrary, whereas the corresponding time unit t_{unit} is the inverse orbital frequency at R_{unit} .

The companion is initiated in a generally eccentric orbit such that, in a Cartesian coordinate system with origin at the center of mass, and (x, y) plane coinciding with the initial disk midplane, both the planet and the line of nodes are on the x axis at time $t = 0$. Parameters associated with the simulations are, the mass ratio of the planet and central star, M/M_\star , the semimajor axis, D , eccentricity, e , and inclination of the planet's orbit, i , to the disk midplane. Finally the run time since initiation with the orbital configuration as described above is also an important parameter as this determines the extent of the warped deformation. Table 1 gives the chosen parameters for various simulations.

In order to compare the simulation results with observation, we have derived the apparent surface brightness distribution associated with the simulation particles. That is the integration along a line of sight of the scattered stellar flux from each particle (Fig. 4). We note that a companion in an inclined orbit breaks the system's azimuthal symmetry. The orientation of the line of sight to line of nodes is

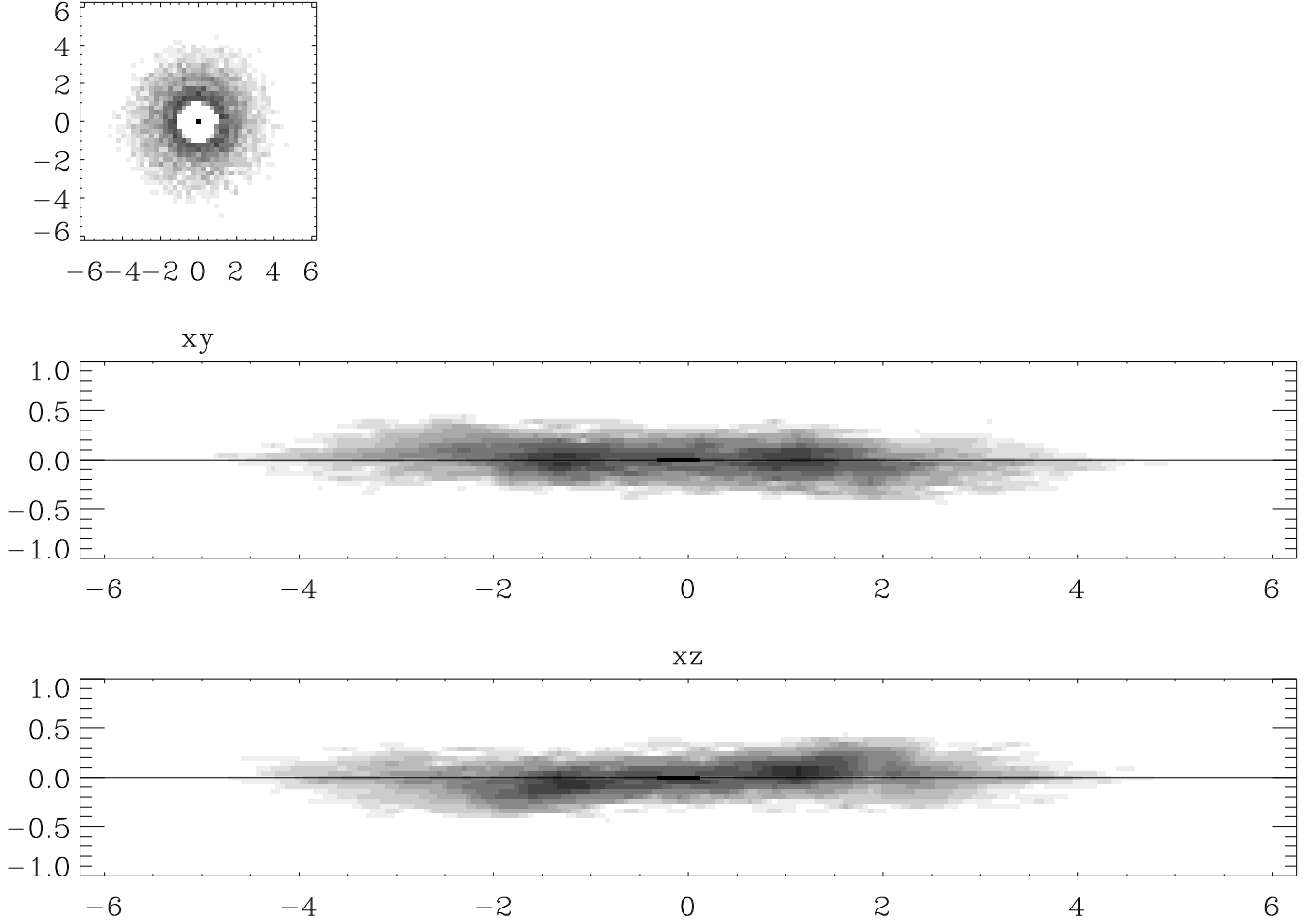


Figure 4. Apparent surface brightness distribution associated with the simulation particles. The represented data set is model 05 at run time = 10^5 . For each projection plane, the axes are scaled in model units

unknown in the case of β Pictoris, and should be considered as a free parameter in fitting the observations.

4 RESULTS

4.1 Simple description of the effect of a companion on the vertical elevation of the disk

Adopting the cylindrical coordinates (r, φ, z) , equivalent to our Cartesian system, the vertical elevation of a razor thin disk moving under the influence of a companion in an inclined circular orbit with small i satisfies

$$\frac{d^2 z}{dt^2} + \Omega_z^2 z = \frac{3 G M D^2}{4 r^4} \sin(2i) \sin(\varphi). \quad (1)$$

Here Ω_z is the frequency of vertical oscillations and the term on the right hand side is the secular vertical acceleration due to the companion. This has been expanded to lowest order in D/r , which becomes an increasingly accurate procedure further out in the disk (Larwood and Papaloizou, 1997). The precession frequency $\omega_p = \Omega - \Omega_z$, is such that $|\omega_p| \ll \Omega$, where Ω is the angular velocity. For particles in near circular

orbits, $\varphi = \Omega t + \text{const.}$, and for small e and i

$$\omega_p = -\frac{3 G M D^2}{4 \Omega r^5}.$$

Using the above in (1), we obtain the approximate solution with zero elevation at $t = 0$,

$$z = -\frac{3 G M D^2 \sin(2i)}{8 \Omega \omega_p r^4} (\sin(\varphi) - \sin(\varphi - \omega_p t)). \quad (2)$$

In this purely kinematic model, the inclined orbit of the companion breaks the midplane symmetry and forces the test particle orbits to precess around the companion's orbital angular momentum axis. If phase mixing due to the r dependence of ω_p is complete ($|\omega_p t| \gg 1$), this process thickens the disk so that the aspect ratio appears to be equal to the orbital inclination. The vertical amplitude of the deformation is thus directly related to the inclination of the companion's orbit.

This relation is verified numerically for the simulation data (Fig. 5). In addition, we note that the apparent amplitude of the warp depends on the orientation of the line of sight (Fig. 6). The observability of the warp is maximized when it (assumed to lie in the outer disk midplane) is at about 30 degrees to the line of nodes.

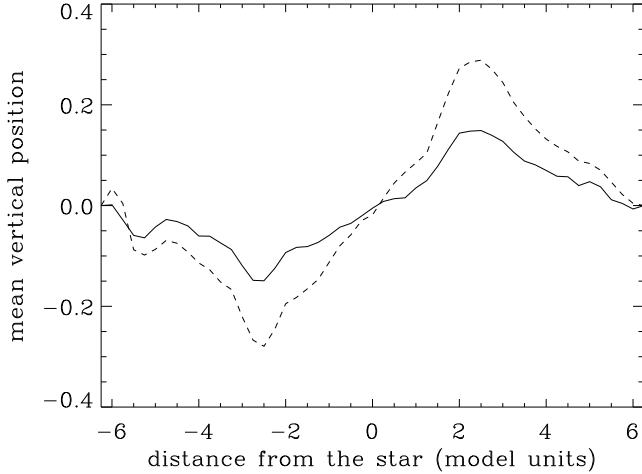


Figure 5. Linear dependence of the amplitude of the warp on the inclination of the companion’s orbit. The axes are scaled in model units. The amplitude of the warp is quantified in the same way as for observational data (see Fig. 2). The effect is twice as large for an inclination of 6 degrees (dashed line, from model 12b), compared to an inclination of 3 degrees (solid line, from model 12), all other parameters equal

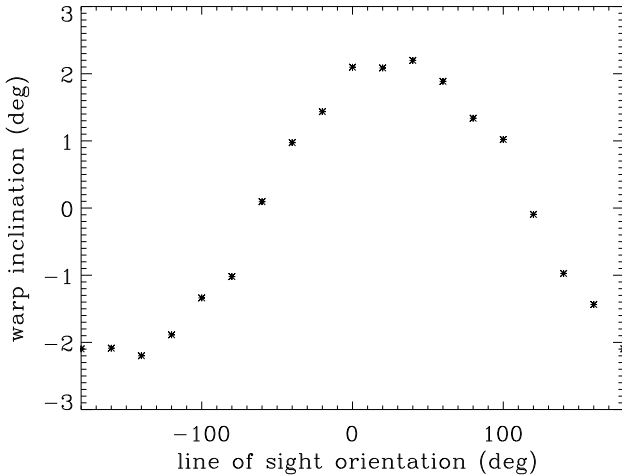


Figure 6. Observability of a warp as a function of the line of sight orientation. The x-axis gives the orientation of the assumed line of sight to line of nodes. The y-axis gives the corresponding apparent inclination of the warp in simulated data (with a 3 degrees inclined companion orbit), measured in the same way as for the observational data (Fig. 2).

4.2 Radial extent of the deformation

A deformation corresponding to a thickened disk is established very fast close to the star and then propagates outwards. As indicated above by (2) the location of the end of the deformation very roughly corresponds to the place where the inverse precession frequency is roughly equal to the run time ($|\omega_p t| \sim 1$). But note that this will overestimate the location of the edge of the deformation because many precession periods are needed to ensure enough phase mixing for the full deformation to be produced. But the number of precession periods required should not depend on radius so

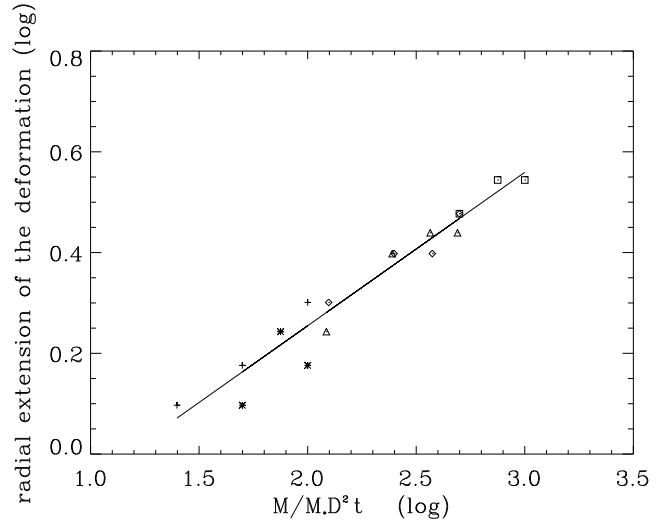


Figure 7. Radial extent of the deformation. The extent of the warp (in model units) is measured in the same way as for the observational data (Fig. 2). It is displayed versus MD^2t in a log-log plot. The simulation data comes from zero eccentricity models (model01: +, model02: *, model04: \diamond , model05: \triangle , model06: \square) and a line of sight orientation of 60 degrees (where the warp observability is unambiguous). Similar results are obtained with other models and orientations. The best fit power law index is numerically measured to be 0.29, in good agreement with the theoretical expectation ($2/7$)

that we expect the scaling relation

$$r \propto (MD^2t)^{2/7}.$$

This form occurs because the propagation rate is driven by the tidal force which is proportional to MD^2 .

The radial dependence of the precession frequency, namely

$$\omega_p \propto MD^2 r^{-7/2},$$

has been checked in the simulations (Fig. 7)

4.3 Companion eccentricity and particle inflow towards the star

We now explore the consequence of a possible eccentricity of the companion orbit. Increasing eccentricities induce very little direct observable effect for a disk seen edge-on (Fig. 8,9). Consequently, this value is poorly constrained by the observations of the β Pictoris disk. Yet, the azimuthal distribution of particles is affected, with the formation of spiral-like features. The stronger the eccentricity, the sharper such features get.

We also notice that the eccentricity of some disk particles gets increased to high values with the result that they are thrown towards the star and end up inside the companion’s orbit. Out of the initial number of 15354 particles with $r > 1.2$, a few get inside the companion orbit ($D = 0.7$) in model 11 ($e = 0.3$), and a few dozen in model 12 ($e = 0.5$).

5 POSSIBLE PARAMETERS FOR THE PERTURBER

The comparison between the simulation results and observations allows derivation of possible parameters for the com-

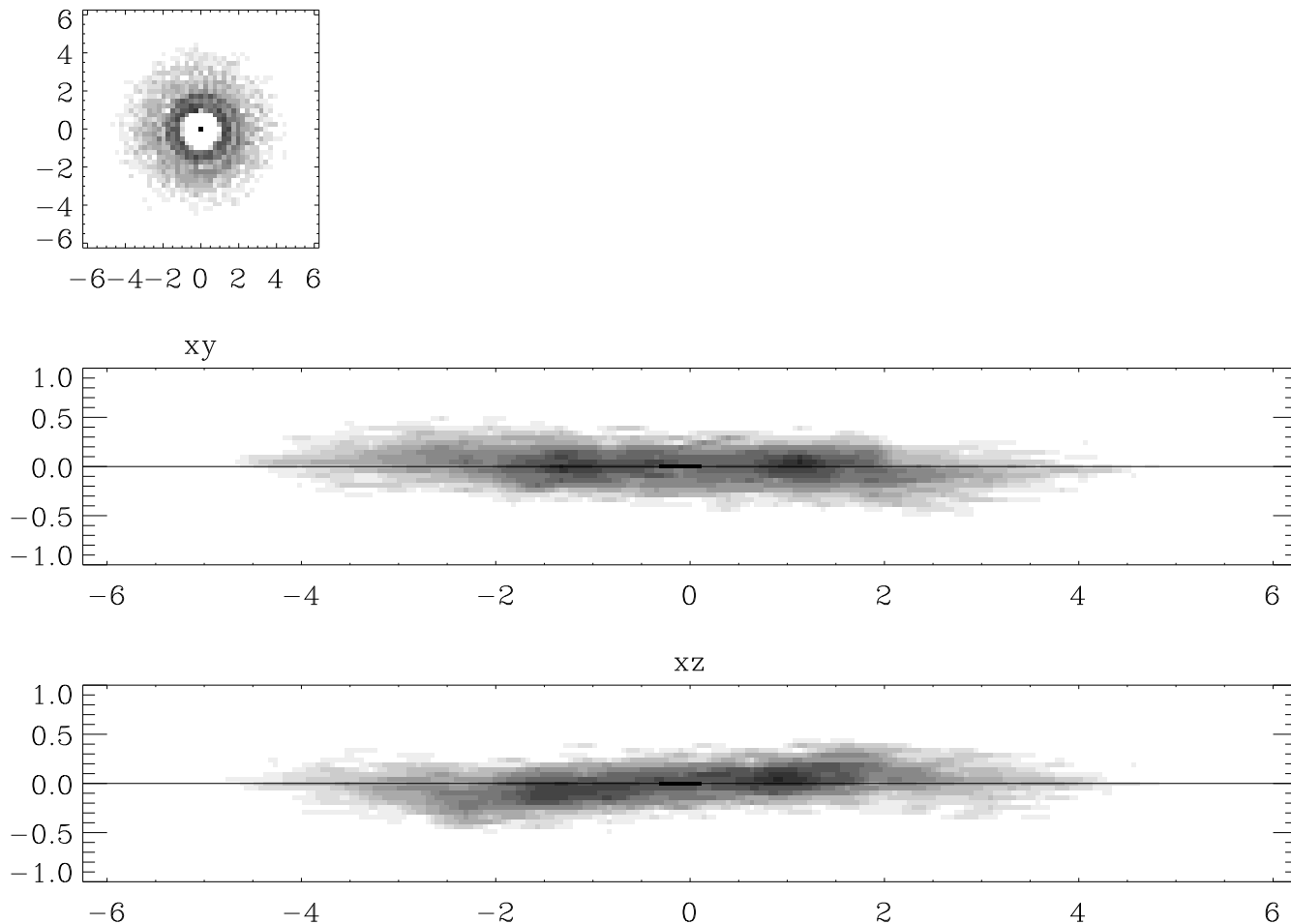


Figure 8. Same as Fig. 4, for model10 at run time $\bar{y}z^2 10^5$: the companion orbit eccentricity is 0.1

panion orbit. First, the observed inclination of 3 degrees requires an orbit inclination of 3-5 degrees to the outer disk midplane, depending on the angle between the line of sight and the line of nodes (these assumed to be coplanar). This angle is poorly constrained but should not lie in the $[-80^\circ, -50^\circ]$ (modulo 180°) range so that the deformation is observable.

Second, the companion orbit is not well constrained by the observation of an edge-on disk, so that it can be considered as a free parameter in the simulations. This could have an important role in feeding material into the inner disk. This, taken together with the general inward migration of the km sized bodies may be related to the cometary infalls observed via spectroscopy, at the rate of about 1000 km -sized bodies per year. Gravitational perturbations are likely to be involved in these processes. A massive companion invoked to explain the imaging data, could then also provide at least part of an explanation for these infalls, as long as its eccentricity is significantly larger than 0.1. We also remark that a moderately large eccentricity is required if an eccentricity pumping mechanism, through mean motion resonances, is supposed to work on particle orbits interior to the planet.

Finally, observations show a radial extension of the warp

of 50 AU. If we arbitrarily choose the model unit $R_{unit} = 10$ AU, then the corresponding model time unit is :

$$t_{unit} = \left(\frac{r^3}{GM_*} \right)^{1/2} = 5.2y.$$

According to the simulations (Fig. 7), the observed extent of the warp ($\log(R/R_{unit}) = 0.7$) requires then the condition :

$$\frac{M}{M_*} \left(\frac{D}{R_{unit}} \right)^2 \frac{t}{t_{unit}} \sim 3000.$$

Assuming that the companion formation is rapid, so that the propagation time of the warp is close to the age of the system, $t \sim 210^8y$. Then a planet with $MD^2 = 10^{-4}M_*(10AU)^2$ can account for the observed warp (Fig. 10). In the framework of these simulations, the companion orbit is interior to the observed disk so that $D \leq 20$ AU. The absence of radial velocity variations larger than about 1 km/s in our spectroscopic data gathered since 1984 implies that $M^2/D_{AU} \leq 5 \cdot 10^{-4}$. Meanwhile, the non direct detection of any close by companion does not constrain further the range of possible parameters. Finally, the possible parameters define a giant planet with a mass $10^{-5} \leq M/M_* \leq 10^{-2}$, located at a corresponding respective distance from the star $20AU \leq D \leq 1AU$. Such a planet may be detected in photometry if it crosses the line

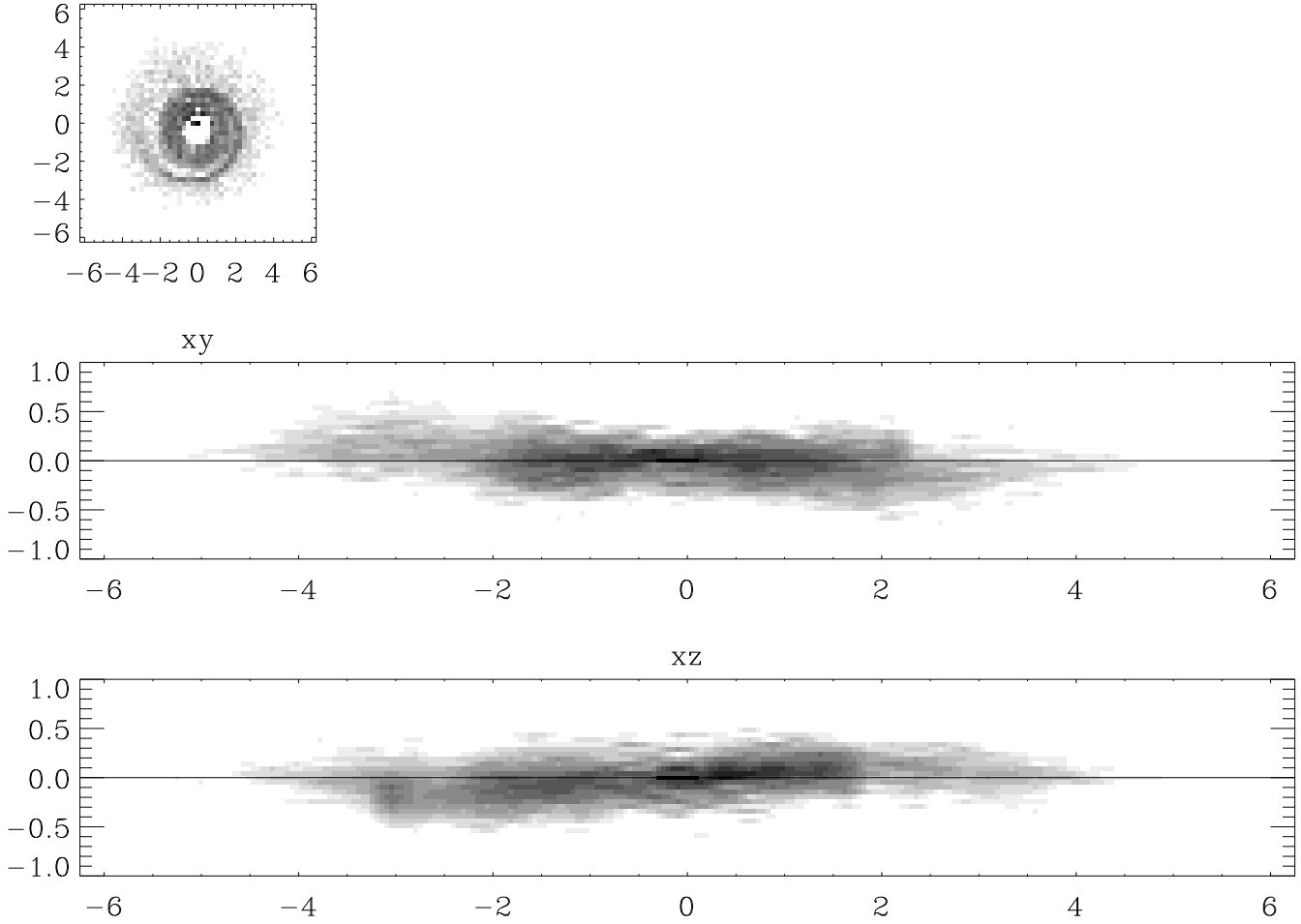


Figure 9. Same as Fig. 4, for modell2 at run time $\bar{y}z^2 10^5$: the companion orbit eccentricity is 0.5

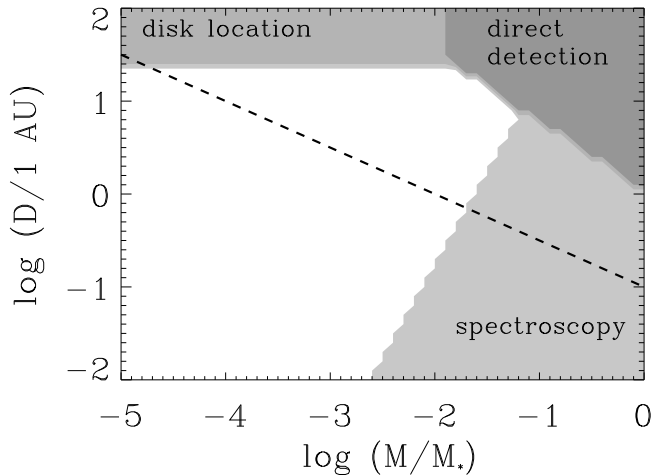


Figure 10. Possible parameters M and D for the gravitational perturber in a log-log diagram. The constraint derived from the extension of the warp is represented by the dashed line. Shaded regions are forbidden because of observational constraints (see text) and the assumption that the companion orbit is inside the disk

of sight, which requires that the earth is in the plane of the planet orbit to within a precision of $0.06^\circ/D_{\text{AU}}$. Actually, Lecavelier et al (1995) propose a Jupiter-like planet to explain short term light variations, which is within the present possible parameter range.

These quantitative results on the possible companion parameters directly depend on the system lifetime, t , which is still unprecisely estimated. However, Crifo et al (1997) derive from the stellar photometry and the new Hipparcos data that the system may not be younger than $10^7 y$. In this case, our corresponding constraint would shift to $MD^2 = 2 \cdot 10^{-3} M_* (10 \text{ AU})^2$. This would restrict the possible parameters to more massive companions ($10^{-3.5} \leq M/M_* \leq 10^{-2}$) between 20 AU and 3 AU.

6 CONCLUSION

From visible as well as NIR imaging observations, the disk around β Pictoris is detected through scattered light from μm sized grains. These grains are short-lived because of destructive collisions and the action of radiation pressure. Assuming that their distribution is the same as an underlying parent population of km-sized bodies, the apparent matter distribution within the disk can be derived from numerical

simulations of collisionless particles. Such simulations are able to reproduce the observed warp in the inner part of the disk as a result of the effect of gravitational perturbations due to a planet in an orbit inclined at 3-5 degrees to the outer disk midplane. Such a planet should be located between 1 and 20 AU, with a corresponding mass respectively between 10^{-2} and $10^{-5} M_{\star}$.

ACKNOWLEDGMENTS

This work was supported in part by EU grant ERB-CBRX-CT93-0329, We are grateful to Alain Lecavelier and Alfred Vidal-Madjar for fruitful discussions on the β Pictoris disk and to N. Hubin and the ESO staff in La Silla for their help in the preparation of and during the ADONIS observations.

REFERENCES

- Artymowicz, P., 1996, in *The Role of Dust in the Formation of Stars*, Eds: R. Siebenmorgen, H. U. Kaufl, Springer
- Artymowicz, P., 1995, In: Ferlet R., Vidal-Madjar A. (eds.) Proc. 10th IAP conf., Frontières, p 47
- Artymowicz, P., 1988, ApJ 335, L79
- Aumann, H.H., 1985, PASP, 97, 885
- Backman, D.E., Paresce F., 1993, in *Protostars and planets III*, university of Arizona press, pp. 1253-1304.
- Beust H., Morbidelli A., 1996, Icarus 120, 358
- Beust, H., Lagrange, A.-M., Plazy, F., Mouillet, D., 1996, A&A , 310, 181.
- Beuzit, J.-L., Mouillet, D., Lagrange, A.-M., A&A , 1997, in press
- Burrows, C.J., Krist, J.E., Stapelfeldt, K.R., 1995, BAAS 187, 32
- Chini, R., et al, 1991, A&A 252, 220
- Crifo, F., Vidal-Madjar, A., Lallement, R., Ferlet, R., Gerbaldi, M., 1997, A&A , accepted
- Kalas, P., Jewitt, D., 1995, AJ 110, 794
- Knacke, R.F., Fajardo-Acosta, S.B., Telesco, C.M., et al, 1993, ApJ 418, 440
- Lagage, P.O., Pantin, E., 1994, Nature 369, 628
- Lagrange, A.-M., et al, 1995, A&A 310, 547
- Lagrange A.M, Ferlet R., Vidal-Madjar A., 1987, A&A 173, 289
- Larwood, J.D., Papaloizou, J.C.B., 1997, MNRAS, 285, 288
- Lecavelier A. et al., 1995, A&A 299, 557
- Lin, D.N.C., Papaloizou, J.C.B., 1985, in *Protostars and planets II*, University of Arizona Press, p 981
- Marcy, G.W., Butler, R.P., 1996, ApJ 464, L147
- Mayor, M., Queloz, D., 1995, Nature 378, 355
- Mouillet, D., Lagrange, A.M., Beuzit, J.L., Renaud, N., A&A , 1997, accepted
- Paresce, F., 1991, A&A 247, L25
- Roques, F., Scholl, H., Sicardy, B., Smith, B.A., 1994, Icarus 108, 37
- Smith B.A., Terrile R.J., 1984, Sci 226, 1421
- Zuckerman, B., Becklin, E.E., 1993, ApJ 414, 793